Toxicon 273 (2026) 108969

Contents lists available at ScienceDirect

Toxicon

journal homepage: www.elsevier.com/locate/toxicon

Selectivity screening of cytotoxicity evoked by viper venoms and their toxins after nanofractionation

Haifeng Xu [a,b], Mátyás A. Bittenbinder [a,b,c], Julien Slagboom [a,b], Nicholas R. Casewell [d], Paul Jennings [a], Jeroen Kool [a,b,*]

[a] Amsterdam Institute of Molecular and Life Sciences, Department of Chemistry and Pharmaceutical Sciences, Faculty of Science, Vrije Universiteit Amsterdam, De Boelelaan 1085, Amsterdam, 1081HV, the Netherlands
[b] Centre for Analytical Sciences Amsterdam (CASA), Amsterdam, the Netherlands
[c] Naturalis Biodiversity Center, Leiden, 2333 CR, the Netherlands
[d] Centre for Snakebite Research & Interventions, Liverpool School of Tropical Medicine, Pembroke Place, Liverpool, L3 5QA, UK

ARTICLE INFO

Handling editor: Bruno Lomonte

Keywords:
Nanofractionation analysis
Viper snake venom
High-throughput venomics
Toxicovenomics
In vitro human cell line

ABSTRACT

Cytotoxicity is a major pathological effect that can occur during snakebite envenoming. To better understand the underlying biochemical and molecular mechanisms behind snake venom-induced cytotoxicity, it is essential to use appropriate *in vitro* tools for bioassaying cytotoxicity evoked by snake venoms. Identifying the toxins causing cytotoxicity is also important in this regard, particularly in the context of developing more effective snakebite treatments. Cytotoxicity induced by venom toxins can result in local pathologies in snakebite victims, which can result in long-term morbidity, and is frequently observed after bites by medically important vipers. In the present study, we optimized and applied an analytical cytotoxicity profiling platform for *in vitro* cytotoxicity assessment of viper venoms. Using four cell lines (RPTEC/TERT1, HepaRG, iPSC-EC, HaCat), we applied an imaging analysis assay together with resazurin reduction to identify the mechanisms of cytotoxicity at the level of cell necrosis, extracellular matrix (ECM) degradation and/or cell apoptosis. Strong cytotoxic peaks are consistent with ECM-associated cytotoxic effects, as reflected by pronounced reductions in cell area and monolayer integrity. These cytotoxicity bioassays were integrated into nanofractionation analytics and high throughput venomics, which allowed for the identification of viper venom cytotoxins at the biological and chemical levels. Venom profiling showed ECM degradation as the main cytotoxic mechanism, except for *Daboia russelii*, which induced necrosis and apoptosis in three cell lines. Cytotoxicity largely disappeared after reversed-phase separation, prompting use of non-denaturing SEC in nanofractionation analytics, which revealed strong cytotoxic peaks for *Bothrops jararaca* and *Calloselasma rhodostoma* in RPTEC/TERT1 cells. The methodology presented here combined analytical and biochemical tools allowing rapid cytotoxicity profiling of viper venom toxins in parallel with toxin identification.

1. Introduction

Snakebite envenoming, a Neglected Tropical Disease, causes more than 100,000 deaths and 400,000 disabilities each year, especially in the global south (Gutierrez et al., 2017; Harrison et al., 2009). Snakebites, particularly those inflicted by viperid snakes, pose a significant global health challenge, particularly in regions with limited access to advanced medical care (Almeida et al., 2025). Vipers are a diverse and widespread family of venomous snakes known for their potent venoms, which can cause a range of life-threatening symptoms during envenoming. When a bite happens, diverse pathological responses occur, with common life-threatening systemic symptoms including coagulopathy, hemorrhage, hypotension, and organ failure (Aglanu et al., 2025). In terms of the results of local cytotoxic effects around the bite site, viperid venoms can cause pain, swelling, muscle and skin necrosis, often leading to debilitating wounds around the bite site (Gutiérrez et al., 2017; Lin et al., 2022). Characterization of the cytotoxins causing these local effects is of importance for the development of targeted strategies to

* Corresponding author. Amsterdam Institute of Molecular and Life Sciences, Department of Chemistry and Pharmaceutical Sciences, Faculty of Science, Vrije Universiteit Amsterdam, De Boelelaan 1085, Amsterdam, 1081HV, the Netherlands.
E-mail address: j.kool@vu.nl (J. Kool).

https://doi.org/10.1016/j.toxicon.2025.108969
Received 2 November 2025; Received in revised form 18 December 2025; Accepted 21 December 2025
Available online 14 January 2026

inhibit venom-induced tissue damage.

The composition of viper venom varies not only between different viper species but also within populations of the same species. These differences are dependent on many factors such as geographical location, age, sex, and habitat (Casewell et al., 2020). Such diversity poses challenges for antivenom production, as antivenoms are typically produced by immunizing large animals such as horses and sheep using venom from a limited number of snake species. This results in not all pathological venom toxins being equally well represented in the pooled venoms used for the immunizations, which can impact the resulting efficacy of treatment against different biting snake species (Williams et al., 2011). When looking closer into venom composition of the viper family, three dominant protein families are recognized, which are the phospholipase A_2s (PLA_2s), the snake venom metalloproteases (SVMPs), and the snake venom serine proteases (SVSPs), followed by some other secondary toxin families which includes the C-type lectins/snaclecs (CTL), disintegrins, and natriuretic peptides (Tasoulis and Isbister, 2017).

Cytotoxicity, which is one of the important pathological effects that can occur during viperid snakebite envenoming, is thought to be mainly caused by venom PLA_2s and SVMPs (Avella et al., 2025; López-Dávila et al., 2021; Szentesi et al., 2025). To better understand the underlying biochemical and molecular mechanisms behind viperid snake venom-induced cytotoxicity, it is important to have appropriate *in vitro* tools for bioassaying cytotoxicity evoked by these snake venoms. Identifying the toxins causing cytotoxicity is also important in this regard, as such target identification can help inform the downstream development of new snakebite treatments. To do so, crude viper venoms first need to be separated and fractionated prior to post-column cytotoxicity assaying. This way, the purified toxins can also be identified using venomics and other mass spectrometric approaches (Slagboom et al., 2020a).

A suitable analytical approach for crude venom separation with post-column bioassaying and parallel toxin identification is nanofractionation analytics, which has been applied to the identification of coagulopathic snake venom toxins (Slagboom et al., 2020b), hemotoxic toxins (Xie et al., 2021), enzymatic PLA_2 toxins (Still et al., 2020), SVMPs (Zietek et al., 2018), and cell damage-associated toxins (Bittenbinder et al., 2023b). Using this analytical approach for profiling venoms for cytotoxicity assessment, Bittenbinder et al. (2023b) integrated an *in vitro* mammalian cell-based assay into the platform to rapidly and robustly test the cytotoxicity of crude venoms and the separated venom toxins. For this, the RPTEC/TERT1 cell line was used with cytotoxicity assays, acquiring the ratio of live cell staining counts, cell area, and resazurin reduction against negative controls, which represent the disruption of the cell membrane, ECM degradation, and cell metabolism loss, respectively. This cytotoxicity assay was integrated within nanofractionation analytics in combination with snake venom proteomics by the High Throughput (HT) venomics approach, recently described by Slagboom et al., enabling characterization of the venom cytotoxins (Slagboom et al., 2023). Collectively, this platform enabled high-throughput profiling of specific cell- and tissue-damaging toxins in snake venoms. Xu et al. (2025) subsequently advanced the platform by assessing the selectivity of cytotoxic responses from crude elapid snake venoms and their fractionated toxins using multiple cell lines. Specifically, the immortalized human proximal tubular cell line (RPTEC/-TERT1), the human liver cell line (HepaRG), induced pluripotent stem cell-derived endothelial cells (iPSC-EC), and the immortalized keratinocyte cell line (HaCat) were used for selective cytotoxicity measurements representative of the kidney, liver, human endothelial tissues, and skin, respectively.

In this study, the approach taken by Xu et al. was applied to investigate the effect of viper venoms on the same cell lines. Six medically important viper venoms were used, from *Bitis arietans, Bothrops jararaca, Calloselasma rhodostoma, Daboia russelii, Echis carinatus*, and *Echis romani*. In addition to crude venom analysis on all four cell lines, nanofractionation analytics were applied to identify directly and indirectly acting cytotoxins on the RPTEC/TERT1 cell line. Because reversed-phase high-pressure liquid chromatography (RP-HPLC) can be denaturing for some venom toxins during separation, size exclusion chromatography (SEC) was used to separate the venom of two viper species (i.e., *Bothrops jararaca* and *Calloselasma rhodostoma*) for cytotoxicity profiling. Subsequently, nanofractionated toxins were exposed to High Throughput (HT) venomics (Slagboom et al., 2023) to identify the constitutive toxins responsible for cytotoxic venom effects.

2. Materials & methods

2.1. Reagents

Chemicals were of analytical grade. Acetonitrile (ACN) and Trifluoroacetic acid (TFA, UHPLC/MS (Ultra-High Performance Liquid Chromatography-Mass Spectrometry) grade) were sourced from Biosolve (Valkenswaard, The Netherlands). Water (Milli-Q plus system, Millipore, Amsterdam, The Netherlands), Hoechst 33342 (Invitrogen, Amsterdam, The Netherlands) and propidium iodide (PI, Sigma p4170, Amsterdam, The Netherlands) were prepared as stock solutions with a concentration of 1 and 2 μg/ml, respectively. Dimethyl Sulfoxide (DMSO, ≥99.9 %, Sigma-Aldrich, Zwijndrecht, The Netherlands), DPBS (Dulbecco's Phosphate-Buffered Saline, Gibco, cat. no. 14190-144, Sigma-Aldrich, Zwijndrecht, The Netherlands), Glutamax (32551-020, Thermofisher, Amsterdam, The Netherlands), Insulin (I9278, Sigma, Amsterdam, The Netherlands), Hydrocortisone hemisuccinate (H2270, Sigma, Amsterdam, The Netherlands), Penicillin/Streptomycin (Pen/Strep; Sigma P4333, Amsterdam, The Netherlands), Fetal Calf Serum (FCS, F6765 Sigma-Aldrich, Zwijndrecht, The Netherlands), Fibronectin (F0895, Sigma-Aldrich, Zwijndrecht, The Netherlands), Resazurin (Thermo Fisher Scientific, Amsterdam, The Netherlands), Iodoacetamide, β-mercaptoethanol and ammonium bicarbonate were from Sigma-Aldrich (Zwijndrecht, The Netherlands). Recombinant Trypsin (EMS0006-4X 100UG) was from Promega Benelux B.V. (Leiden, The Netherlands). The 96-well plates (F-bottom, with lid, sterile, Cat-No. 655,180, CELLSTAR$^{@}$) were from Greiner Bio-One (Amsterdam, The Netherlands).

2.2. Venoms

Bothrops jararaca (jararaca, captive bred), *Calloselasma rhodostoma* (Malayan pitviper, captive bred), *Echis romani* (Roman's saw-scaled viper, Nigeria) and *Echis carinatus* (Indian saw-scaled viper, India) venoms were stored lyophilized at 4 °C. These were provided by the Centre for Snakebite Research and Interventions Herpetarium (Liverpool School of Tropical Medicine, UK). Note that the Indian *E. carinatus* venom was collected from a specimen that was inadvertently imported to the UK via a boat shipment of stone, and then rehoused at LSTM on the request of the UK Royal Society for the Prevention of Cruelty to Animals (RSPCA). *Bitis arietans* (puff adder, captive bred) and *Daboia russelii* (Russell's viper, locality unknown) were provided by the National University of Singapore. The venom stock solutions of the crude venoms (1 ± 0.1 mg/mL) were prepared in water before analysis, and then aliquoted and stored at −80 °C until use. All venoms were acquired prior to the implementation of the Nagoya protocol.

2.3. Cell culturing and mammalian cellular assays

2.3.1. Cell culture

All cells from the four cell lines used were cultured at 37 °C in a 5 % (v/v) CO_2 humidified atmosphere with medium refreshment every two days until confluence. For medium preparation, RPTEC/TERT1 (Evercyte GmbH, Vienna (Wieser et al., 2008)) were cultured in a mixture of Dulbecco's modified Eagle's medium (DMEM; catalog no. 11966-025; Invitrogen, Leiden, The Netherlands) and Ham's F-12 nutrient mix (catalog no. 21765-029; Invitrogen, Leiden, The Netherlands) in a ratio

of 1:1 supplemented with 2 mM glutamax, 5 ng/ml insulin, 5 μg/ml transferrin, 5 ng/ml sodium selenite, 100 U/ml penicillin and 100 μg/ml streptomycin, 10 ng/ml epithelial growth factor and 36 ng/ml hydrocortisone (Aschauer et al., 2013).

HepaRG cells (human HepaRG cells (Biopredic International, St Grégoire, France) were maintained in Williams' E medium supplemented with 2 mM glutamax, 100 U/ml penicillin, 100 μg/ml streptomycin, 5 μg/ml insulin and 50 μM hydrocortisone hemisuccinate, and 9 % FCS. An additional 1.7 % DMSO was added to the medium to obtain differentiated cells with the activation of Cytochrome P450s (CYT P450s). One day before treatment, cells were fed with the same medium in the absence of DMSO and FCS. This medium was also used for treatments with crude venom or nanofractionated venom toxins (Hofmann et al., 2018).

Induced Pluripotent Stem cell-derived endothelial cells (iPSC-ECs) were differentiated from human iPSC cells as previously described (Christensen et al., 2019). The protocol uses a 3-step differentiation over 6 days, with the last step including forskolin and VEGF (Vascular Endothelial Growth Factor) stimulation. We deviated from the protocol by purifying the cells with CD31 (PECAM) magnetic bead sorting instead of CD144 (VE-cadherin). CD31 positive cells were cultured on fibronectin-coated plates and maintained in VascuLife endothelial medium complete kit (LifeLine Cell Technology, LL-0003) containing VEGF165 (StemCell Technologies, 78073.1, Amsterdam, The Netherlands), SB-431542 (10 μM, TGF-beta inhibitor, M1794, Amsterdam, The Netherlands) and 10 % FCS and Pen/Strep. Cells were not allowed to reach confluence. To coat the well plates, fibronectin was thawed and allowed to reach room temperature, and then diluted with DPBS (Reagent above) at a 1:5 ratio. Then, 70 μL of this diluted fibronectin solution was added to each well in the 96-well plate and left at room temperature for 1h in a flow cabinet, after which the solution was removed by pipette. The plate was washed with 100 μL DPBS three times (coated plates were stored in the refrigerator for up to two weeks before use).

Immortalized keratinocyte cells (HaCat, Vrije Universiteit Amsterdam, The Netherlands) were cultured in DMEM with glutamax, 10 % FCS, and 1 % Pen/Strep. Cells grew to confluence in three days.

2.3.2. Cell assays

Cellular morphological data was collected by a confocal Operetta CLS high content imager (HCI) (PerkinElmer, Waltham, MA, USA) and analyzed by Harmony software 4.8 (PerkinElmer, Waltham, MA, USA). Four types of filter channels consisting of two fluorescence channels (Hoechst and PI), a brightfield channel (white light), and a digital phase contrast (DPC) channel were applied with the machine-learning technology, which can generate an image analysis algorithm for qualitative and quantitative analysis (Bode et al., 2019; Selinummi et al., 2009).

The first fluorescent assay was applied for the detection of cell permeability using the cell-permeable dye Hoechst 33342 and the cell-impermeable dye propidium iodide (PI) under Ex355-385 nm & Em 430–500 nm and Ex530-560 nm & Em570-650 nm respectively. For crude venom, venoms were firstly dissolved with cell medium mixed with fluorescent reagent (Hoechst: 1 to 20000; PI: 1 to 10000) and serially diluted in the concentrations of 100, 33.3, 11.1, 3.3, 1.1 μg/ml in clean 96 well plates, then the plates were incubated for 10 min at 37 °C. The relevant daily culture medium was used for the different cell lines. For nanofractionated venom, 100 μl of medium mixed with Hoechst 33342 and PI at the same ratio as in crude venom was added to each well in 96-well plates containing nanofractionated toxins, and then incubated for 10 min at 37 °C. For exposure, the medium in the plate cultured with the cells was first removed and then replaced with the medium containing serially diluted crude venom or nanofractionated venom. The plates were then incubated for 24 h at 37 °C and then measured using the HCI. Indirect cytotoxicity was also measured for all the crude venoms and several nanofractionated venoms, by performing the same experiments in the presence of extra egg yolk. In detail, egg yolk was dissolved with the cell-cultured medium containing Hoechst and PI at an end concentration of 1.75 mg/mL, as previously described (Xie et al., 2021). For data acquisition, combining the brightfield channel (white light) and digital phase contrast (DPC) channel contributed to detecting the surface area of the cell monolayer with enhanced contrast and low background noise from the two fluorescence channels, which allowed for readout and calculation of cell area. The y-axis of the live cell number for each dilution was then calculated based on the result of the Hoechst-stained cell number, subtracting the PI-stained cell number for each well of the 96-well plates used.

After measurement in HCI with Hoechst/PI assay, the second fluorescent assay, the resazurin reduction assay, was performed on the same well plate, which was then replaced with fresh culture medium. In detail, 5 μl of 20 mM Resazurin solution was added to each well and incubated for 1 h at 37 °C. Next, a CLARIOstar Plus reader (BMG Labtech, Ortenberg, Germany) was used to measure the signal of the whole plate at 540 nm excitation and 590 nm emission. Resazurin is a soluble blue dye that is reduced to the highly fluorescent red-colored resorufin by cellular reductase activity in living cells. The y-axis of resazurin reduction induced by venoms/toxins could be calculated based on the fluorescence intensity of each well of the 96-well plates used and was used to monitor cell metabolism (Aleshin et al., 2015). The positive control and negative control were treated with 1 % Triton X-100 (Sigma, Amsterdam, The Netherlands) and regular culture medium, respectively.

From the above-described bioassays, cytotoxicity was presented as the ratio of live cell count and cell area via the Hoechst/PI assay, and resazurin reduction from the resazurin reduction assay in each well against the corresponding values measured in the negative controls. The cell permeability disruption was identified both by the statistics of readout of live cell counts and manual identification of morphology data in this study. That was done manually because many viper venoms can degrade the cell monolayer, resulting in cell detachment from the bottom of the well of the well plate, thereby getting out of the focus of the microscope of HCI, which then prevents microscope-based counting of total cell numbers. Indirect cytotoxicity was also assessed and was measured using the same analytical and bioassaying procedures but with the addition of egg yolk emulsion (final concentration 1.75 mg/mL) mixed with culture medium and venom or separated toxins before exposure to cells. In the case of the nanofractionated toxins, assay results from the cytotoxicity assays were plotted as bioactivity chromatograms by plotting assay readout on the y-axis vs. time of toxin fractionation on the x-axis in GraphPad Prism 9 (GraphPad, California, USA). The positive control was labeled and plotted on the right side of each bioassay chromatogram. All cellular assay data was plotted as means ± SEM unless otherwise specified. Statistical analysis was performed using GraphPad Prism. Intergroup differences for continuous variables were assessed by one-way ANOVA, using Dunnett's post-test to determine the significance of differences between control and treated groups.

2.4. RP-HPLC & SEC separations followed by nanofractionation

2.4.1. RP-HPLC

50 μL crude venom solutions (1 mg/mL) were injected with a Shimadzu SIL-20AC autosampler (Shimadzu Benelux, s-Hertogenbosch, The Netherlands) and then separated by a 100 × 4.6 mm Waters XBridge Peptide BEH 300 C18 analytical column (5-μm particle size, 300 Å pore size, Waters, Etten-Leur, The Netherlands) in a column oven of 30 °C (Shimadzu CTD-10AC). The column effluent (flow rate of 0.5 ml/min) was sent to a Shimadzu SPD-20A Prominence diode array detector (wavelengths of 220 nm) before going to a flow splitter. The analytical mobile phase gradient was controlled by two Shimadzu LC-20AB pumps with Mobile phase A (MQ; ACN; TFA, 98 %; 2 %; 0.1 %) and mobile phase B (ACN; MQ; TFA, 98 %; 2 %; 0.1 %). All the settings of the system were controlled with Shimadzu Lab Solutions software (v. 5.117, Amsterdam, The Netherlands). The RP-HPLC gradients used in this study

were first optimized for each venom, and the optimized gradient information can be found in Supporting Information 1.5. The fractions were collected at a resolution of 20 s/well onto 96-well plates. All the collected toxins in the plates were subsequently vacuum centrifuged to dryness overnight using a Christ Rotational Vacuum Concentrator (RVC 2–33CD plus, Zalm en Kipp, Breukelen, The Netherlands) operated with a −80 °C cooling trap. The dried plates were stored at −20 °C until bioassaying.

2.4.2. SEC

After screening of nanofractionated viper venoms with the RPTEC/TERT1 cell line, it was found that the notable cytotoxicity measured for the crude venoms was lost, which may be caused by the high organic solvent concentrations used during separation in combination with a low eluent pH. Therefore, we investigated another, non-denaturing, separation method (i.e., Size Exclusion Chromatography; SEC), in a similar manner as used by Bittenbinder et al. (2023a) and Wachtel et al. (2023). In this approach, the mobile phase used consisted of the non-volatile salt buffer DPBS. Two venoms (*B. jararaca* and *C. rhodostoma*, 5.0 mg/ml) were fractionated onto 96-well plates using SEC on a Shimadzu HPLC system controlled with the Shimadzu Lab Solutions software. The venom samples were injected with a Shimadzu SIL 20AC Prominence autosampler utilizing a 20 µL injection volume. Subsequent separation was performed on a Sepax Zenix SEC-300 column (300 Å, 5 µm, 4.6 mm × 300 mm, Sepax Technologies, USA) in a Shimadzu CTO-10AC VP column oven set to 30 °C. The mobile phase consisted of 100 % DPBS (GibcoTM Dulbecco's phosphate-buffered saline (no calcium, no magnesium, pH 7.0 to 7.3) using an isocratic elution over 20 min and a flow rate of 0.35 mL/min. The elution of the toxins was monitored using a Shimadzu SPD-20A Prominence ultraviolet (UV)/Vis detector set at 220 and 280 nm. Between each run, the system was flushed using a solvent loop that was added to the pump system (with a mixture of 20 % 2-propanol and 80 % MQ), which was used to flush the system and ensure proper toxin separation. Following the SEC column, the samples were collected as 12-s fractions in a 96-well flat-bottom plate (Greiner Bio-One) for 18 min, using a 6-min delay after the start of each subsequent run. For fractionation, we used a Gilson ASTED-XL autosampler rebuilt as a fraction collector, which was controlled by Ariadne software (in-house written software, v1.08j). This resulted in the collection of 60 wells, each with ~60 µL collected sample fractions. The plates were kept at 4 °C until use. Upon use, we transferred the venom fractions (in DPBS) to a separate 96-well plate, after which these were supplemented to a total volume of 100 µL (in an 80 % ((venom fractions in PBS)) to 20 % ((growth medium)) ratio).

Since there are small time differences in eluted toxins for arriving at UV and fractionation, the UV and fractionation times needed to be aligned. This was done by measuring the retention time of the thrombin inhibitor argatroban in UV, and by fractionating the inhibitor on a well plate followed by performing a coagulation bioassay as described by Mladic et al. (2016). The bioassay chromatogram resulting from the coagulation bioassay will give a negative peak for argatroban from which a retention time can be measured. By measuring the differences in retention time between UV and the coagulation bioassay, the delay times could be calculated, which were then used to align the UV and bioassay data presented in this study. The column temperature for RP-HPLC separations was set at 30 °C. Moderate elevation of column temperature is commonly applied in venom proteomics and protein chromatography to improve mass transfer, peak shape, and chromatographic reproducibility. Under gradient elution conditions, increased temperature reduces analyte–stationary phase interactions and facilitates elution at lower organic solvent concentrations. At this temperature, no significant unfolding of venom toxins is expected, as these proteins are inherently stable at temperatures approaching mammalian body temperature.

2.5. HT venomics for toxin identification

High-throughput (HT) venomics was previously developed by Slagboom et al. (2023) and applied in this study to identify cytotoxins. In short, 120 µl fractions from the LC separations of the venoms were collected in wells of 96-well plates with the FractioMate in the same manner as done for collecting fractions for the cytotoxicity bioassaying. Samples were then transferred to 384-well plates and vacuum centrifuged to dryness overnight. Next, each fraction in the wells underwent tryptic digestion followed by nanoLC-MS/MS analysis according to Slagboom et al. (2023).

Chromatographic separation was conducted using an UltiMate 3000 RSLCnano system (Thermo Fisher Scientific, Ermelo, The Netherlands). The autosampler, which accommodates three microplates, was operated in partial-loop injection mode to enable direct sample loading from 384-well plates. The injection volume was fixed at 1 µL, with subsequent separation performed on an Acclaim PepMap 100 C18 analytical column (150 mm × 75 µm, 2 µm particle size, 100 Å pore size) coupled to an Acclaim PepMap 100 C18 trapping column (5 mm × 0.3 mm, 5 µm particle size, 100 Å pore size); both columns were purchased from Thermo Fisher Scientific. The mobile phase consisted of two eluents: Eluent A (98 % water, 2 % acetonitrile [ACN], 0.1 % formic acid [FA]) and Eluent B (98 % ACN, 2 % water, 0.1 % FA). The separation gradient for peptide digests was programmed as follows: an initial isocratic hold at 1 % B for 3 min; a linear gradient ramp to 40 % B over 7.5 min; a rapid linear increase to 85 % B within 0.1 min; an isocratic elution at 85 % B for 0.7 min; a linear re-equilibration to 1 % B over 0.2 min; and a final column equilibration at 1 % B for 3.7 min. The column oven temperature was maintained at 45 °C throughout the run.

Mass spectrometric detection was carried out on a maXis QTOF mass spectrometer (Bruker Daltonics, Germany) equipped with a Bruker CaptiveSpray ion source operated in positive-ion mode. The source parameters were set as follows: source temperature 150 °C, capillary voltage 1.2 kV, dry gas flow rate 3.0 L/min, and nanoBooster pressure 0.20 bar. Full-scan mass spectra were acquired at a frequency of 2 Hz over an m/z range of 50–3000. Tandem mass spectra were generated by collision-induced dissociation (CID) in data-dependent acquisition mode. Instrument control and data processing were performed using Bruker Compass software (version 3.0).

The resulting proteomics data was analyzed using Mascot database searching. Finally, the analyzed data was converted into an Excel file using an in-house written R script. The data was finally plotted into so-called protein score chromatograms with the retention time of fractionation on the x-axis versus the protein score on the y-axis.

3. Results and discussion

The objective of this study was to optimize and apply a methodology for obtaining the cytotoxicity profiles of viper snake venoms against different tissue-representative cell lines, and to facilitate identification of responsible venom cytotoxins. The four cell lines included in this study were RPTEC/TERT1, HepaRG, iPSC-EC, and HaCat, which are models for assessment of cytotoxicity to the following tissues: kidney, liver, endothelium and skin. In addition to crude venom cytotoxicity assessments, the analytical workflow also included venom nanofractionation coupled to RPLC (reverse phase liquid chromatography) and SEC, followed by post-column cytotoxicity screening of fractionated toxins for the cell lines included in the study, and HT venomics for toxin identification. For each cell assay, the three readouts used were the ratio of live cell counts, cell area, and resazurin reduction against negative controls, which together represent cytotoxicity potency measured as cell permeability disruption, ECM degradation, and cell metabolism loss, respectively.

3.1. Cytotoxicity profiling of crude viper venoms against the four cell lines

3.1.1. Renal proximal tubule RPTEC/TERT1 cells

The cytotoxicity of *B. arietans*, *B. jararaca*, *C. rhodostoma*, *D. russelii, E. carinatus* and *E. romani* was assessed after exposure of cultured RPTEC/TERT1 cells in 96 plates with serially diluted crude venoms (0, 1.1, 3.3, 11.1, 33.3, and 100 μg/ml final concentrations were used) for 24 h. Similar cytotoxicity effects representative of ECM degradation were observed for most of the tested vipers, except for *D. russelii* (Fig. 1). Cell plasma membrane and cell viability were stable after being exposed to all viper venoms tested. The only venom that did not show any significant cytotoxicity on initial testing was *D. russelii*, even at the maximum tested concentration of 100 μg/ml. A previous study investigating this venom showed lysis of vascular wall cells and disruption of their confluent monolayer (or ECM degradation) for renal epithelial cells (LLC-PK_1), at higher venom concentrations (>600 μg/ml) (Willinger et al., 1995). When testing indirect cytotoxicity effects in the presence of egg yolk emulsion (Fig. S1), we observed increased cell permeability disruption and intensified ECM degradation in all venoms at lower venom concentrations compared to the direct cytotoxicity effects observed, except for *D. russelii*, which only expressed cell permeability disruption. Resultant cell viability remained stable for most viper venoms, except for *B. jararaca,* which yielded a slight decrease at the highest venom concentration tested. An elaborate description of the cytotoxicity readouts can be found in Supplementary material 1.1.

3.1.2. Liver hepatocyte HepaRG cells

The HepaRG cell line was tested with the same venoms at the same concentrations and using the same screening procedure and data analysis as for the RPTEC/TERT1 cell line. Unlike the direct effects observed in the RPTEC/TERT1 cell line, the HepaRG cell line presented a more sensitive cytotoxicity reaction to the viper venoms. All investigated venoms, except *D. russelii*, induced cell permeability disruption, ECM degradation, and cell viability loss, albeit with different potencies (Fig. 2). Cell permeability disruption and cell viability loss was only observed in the cytotoxicity screening results of *D. russelii* venom at the higher venom concentrations of 33.3 and 100 μg/ml (Fig. 2). As with the RPTEC/TERT1 cell line, indirect cytotoxicity effects measured by cell permeability disruption were increased in the presence of egg yolk (Fig. S2). ECM degradation was enhanced with the venoms of *B. arietans*, *B. jararaca,* and *E. carinatus* (Fig. S2). An elaborate description of the cytotoxicity readouts can be found in the Supplementary material 1.2.

3.1.3. Human umbilical vein endothelial iPSC-EC cells

The iPSC-EC cell line mimics human endothelial cells which likely are also affected by hemolytic effects of viper snake venoms, leading to hemorrhage (Du et al., 2006). This cell line therefore likely presents a useful model for investigating endothelial cell damage by venoms. The iPSC-EC cell line was investigated with the same venoms, concentrations, screening procedure, and data analysis. Similar to the cytotoxicity profiles measured for the HepaRG cell line, all the viper venoms except *D. russelii* resulted in cell permeability disruption, ECM degradation, and cell viability loss (Fig. 3). Indirect cytotoxicity effects gave the most enhanced effects of all cell lines tested. At very low venom concentrations, cytotoxicity was observed with the venoms of *B. jararaca*, *C. rhodostoma*, *E. carinatus* and *E. romani* resulting in the most potent indirect cytotoxicity as determined by readouts of cell permeability disruption, ECM degradation, and cell viability loss (Fig. S3). For *D. russelii,* only significant cytotoxicity readouts for cell permeability disruption and cell viability loss were observed. Given that egg yolk and more specifically phospholipids can induce hemolytic effects simulated by PLA_2 toxins (Xie et al., 2021), this might be the main cause of the increased cytotoxicity observed in iPSC-EC cells. An elaborate description of the measured cytotoxicity readouts can be found in the

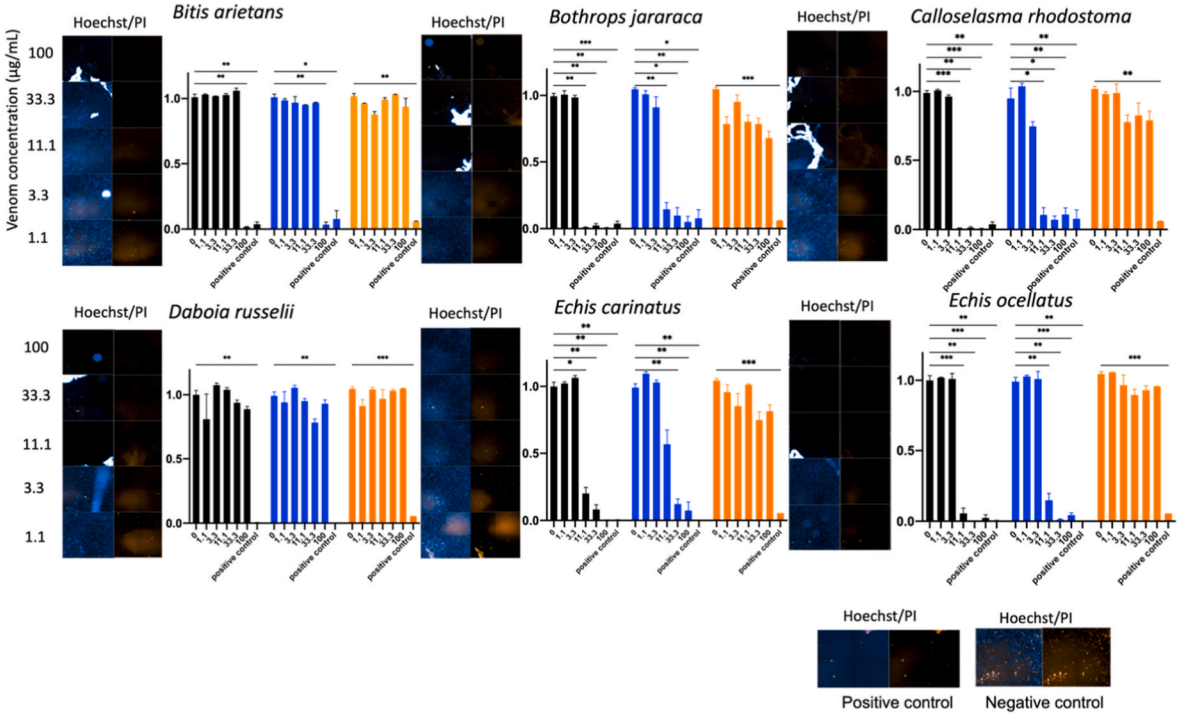

Fig. 1. Morphological images and three readouts for direct cytotoxicity assessment of crude venom on RETEC/TERT1 cells. Serial dilutions of the venoms (0, 1.1, 3.3, 11.1, 33.3, and 100 μg/mL) included in this study were investigated: black, ratio of live cell counts vs negative control (NC); blue, ratio of cell area vs NC; orange, ratio of resazurin reduction vs NC. Error bars show the mean ratio plus standard error. * highlights a statistically significant difference when compared to the negative control, PC represents the positive control, and PI means Propidium Iodide. Statistical testing was performed by two-way ANOVA, n = 3, *: p (Confidence Interval) < 0.05, **: $p < 0.005$, ***: $p < 0.0005$. All the bar chart share the same y-axis units, representing the ratio percentage (%) between the tested wells and the negative control wells.

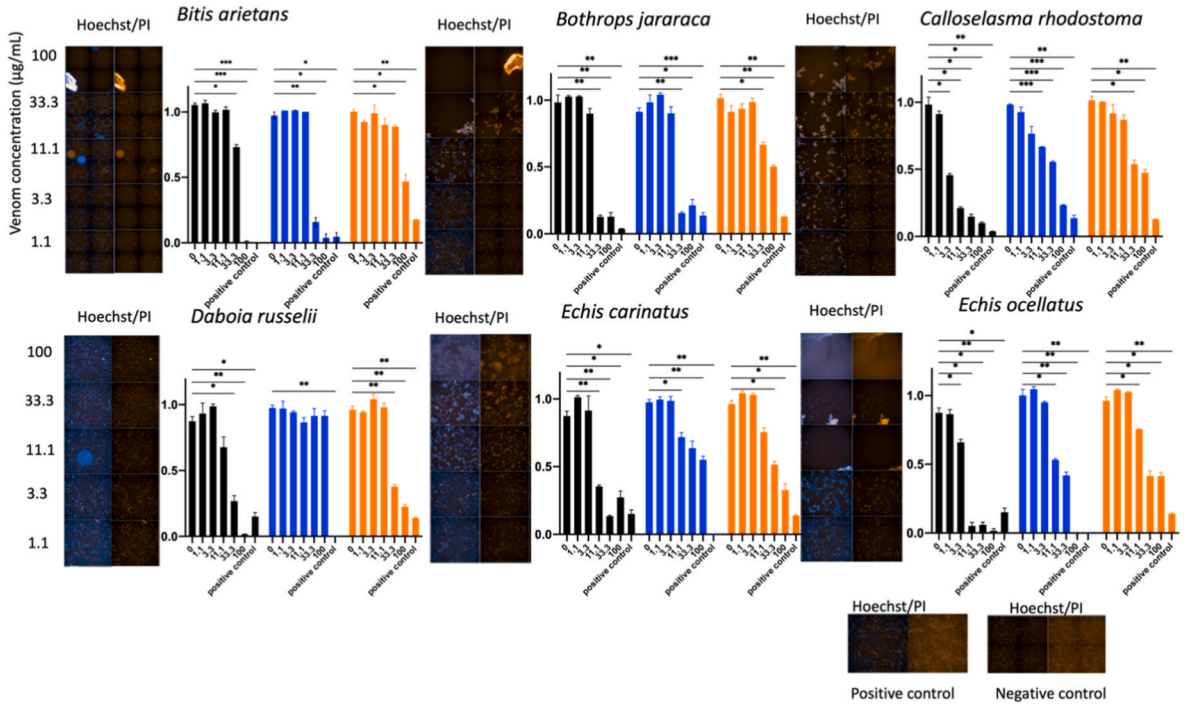

Fig. 2. Morphological images and three readouts for direct cytotoxicity assessment of crude venom on HepaRG cells. Serial dilutions of the venoms (0, 1.1, 3.3, 11.1, 33.3, and 100 µg/mL) included in this study were investigated: black, ratio of live cell counts vs negative control (NC); blue, ratio of cell area vs NC; orange, ratio of resazurin reduction vs NC. Error bars show the mean ratio plus standard error. * highlights a statistically significant difference when compared to the negative control, PC represents the positive control, and PI means Propidium Iodide. Statistical testing was performed by two-way ANOVA, n = 3, *: p (Confidence Interval) < 0.05, **: $p < 0.005$, ***: $p < 0.0005$. All the bar chart share the same y-axis units, representing the ratio percentage (%) between the tested wells and the negative control wells.

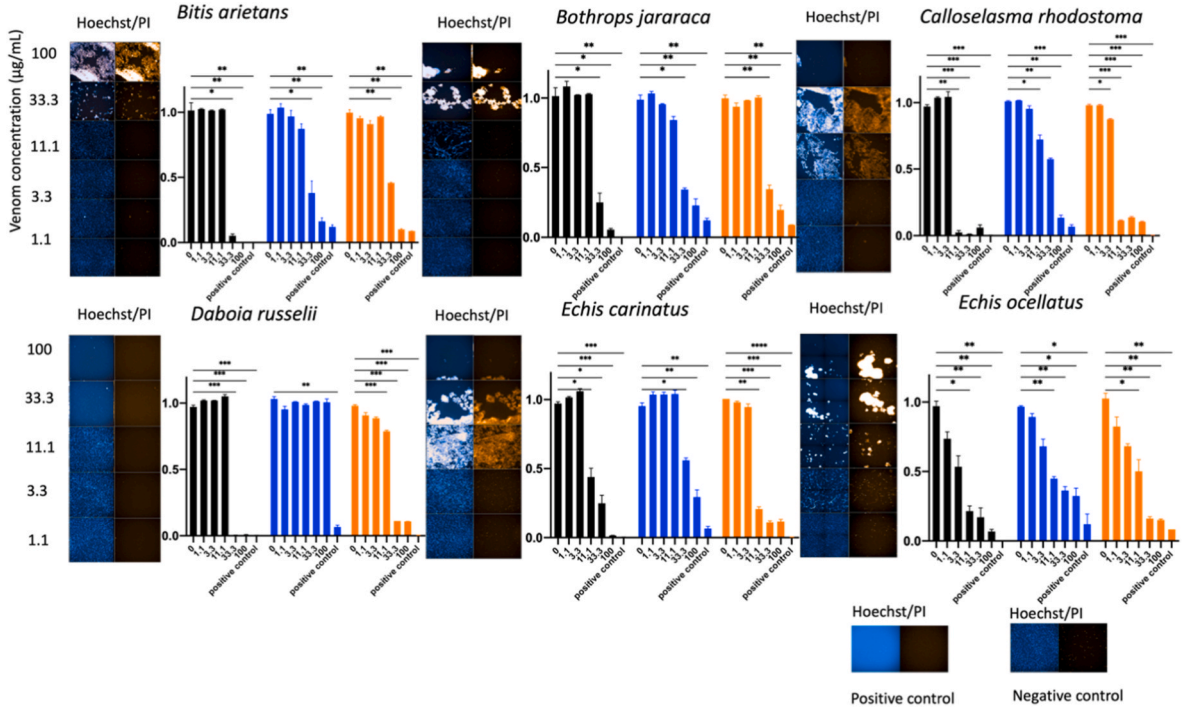

Fig. 3. Morphological images and three readouts for direct cytotoxicity assessment of crude venom on iPSC-EC cells. Serial dilutions of the venoms (0, 1.1, 3.3, 11.1, 33.3, and 100 µg/mL) included in this study were investigated: black, ratio of live cell counts vs negative control (NC); blue, ratio of cell area vs NC; orange, ratio of resazurin reduction vs NC. Error bars show the mean ratio plus standard error. * highlights a statistically significant difference when compared to the negative control, PC represents the positive control, and PI means Propidium Iodide. Statistical testing was performed by two-way ANOVA, n = 3, *: p (Confidence Interval) < 0.05, **: $p < 0.005$, ***: $p < 0.0005$. All the bar chart share the same y-axis units, representing the ratio percentage (%) between the tested wells and the negative control wells.

Supplementary material 1.3.

3.1.4. Dermal keratinocyte HaCaT cells

Lastly, the HaCat cell line was tested under the same conditions as used for the other cell lines. For this cell line most venoms induced cell permeability disruption, ECM degradation, and cell viability loss at different concentrations (Fig. 4). Like with the other cell lines tested, the activity of *D. russelii* venom was restricted to only inducing cell permeability disruption and cell viability loss. For the indirect effects measured, our results differed to the other cell lines tested, with only *E. carinatus* (Fig. S4) venom inducing partially enhanced cytotoxicity compared to the direct effects, which were observed as enhanced cell permeability disruption and ECM degradation. An elaborate description of cytotoxicity readouts can be found in the Supplementary material 1.4.

3.1.5. Summary of crude venom screening

Variability in absolute PI signal intensity was observed across conditions, including occasional elevated PI signal in negative control wells. All staining concentrations, incubation times, and imaging parameters were strictly controlled. Such variability is a known feature of membrane-impermeant dyes and can arise from transient membrane perturbation or cell handling effects. Importantly, cytotoxicity interpretation in this study relies on combined multiparametric analysis rather than PI signal alone, ensuring robust relative comparison of venom-induced effects.

The different cytotoxicity profiles observed in the four cell lines were characterised by different cytotoxicity potencies and resulting effects, suggesting variability in terms of cell sensitivity to viper venoms. For direct cytotoxicity (Table S1), the most potent cytotoxicity was observed in the iPSC-EC cell line which is an interesting finding leading to the potential of using this cell line as *in vitro* tool for investigating hemotoxicity (such as hemorrhage) (Gutiérrez et al., 2016). Similar cell viability loss and cell apoptotic damage have been observed in previous research (Gutiérrez et al., 2005). Previous studies contributed by looking at the mechanism of ECM degradation as the result of detachment of cells and vascular permeability change (Baldo et al., 2010). In addition to these studies, our results showed that both the permeability of the endothelial cell membrane and cell viability were also affected. Previously, a synergistic effect of acidic PLA_2s and SVMPs was observed by Soledad et al. (Bustillo et al., 2015), while a detaching effect of endothelial cells cultured *in vitro* and caused by a purified SVMP from *Bothrops alternatus* venom was enhanced by purified acidic PLA_2. In this study, ECM-associated cytotoxicity was inferred from phenotypic readouts obtained using high-content imaging, particularly pronounced reductions in cell area and monolayer integrity. In our previous work, such imaging-based phenotypes were experimentally linked to SVMP-rich venom fractions through nanofractionation and venomics approaches (Bittenbinder et al., 2023b; Xu et al., 2025). However, the present study does not directly quantify ECM degradation products. Accordingly, the observed cell area reduction should be interpreted as being consistent with ECM-associated cytotoxic effects rather than as direct biochemical proof of ECM degradation. Definitive confirmation would require targeted proteomic analysis of ECM-derived peptides in culture supernatants, which was beyond the scope of the present study.

Egg yolk was included as an exogenous phospholipid source to enhance detection of indirect cytotoxic effects, particularly those mediated by PLA_2 toxins. In previous studies using this analytical cytotoxicity profiling platform, the presence of egg yolk has been shown to sensitize the assay toward PLA_2-driven membrane-associated toxicity, thereby enabling discrimination between direct cytotoxic effects and indirect mechanisms involving membrane disruption and downstream metabolic dysfunction. The increased cytotoxicity observed in egg yolk-containing samples is therefore consistent with established PLA_2-mediated mechanisms and provides complementary information rather than

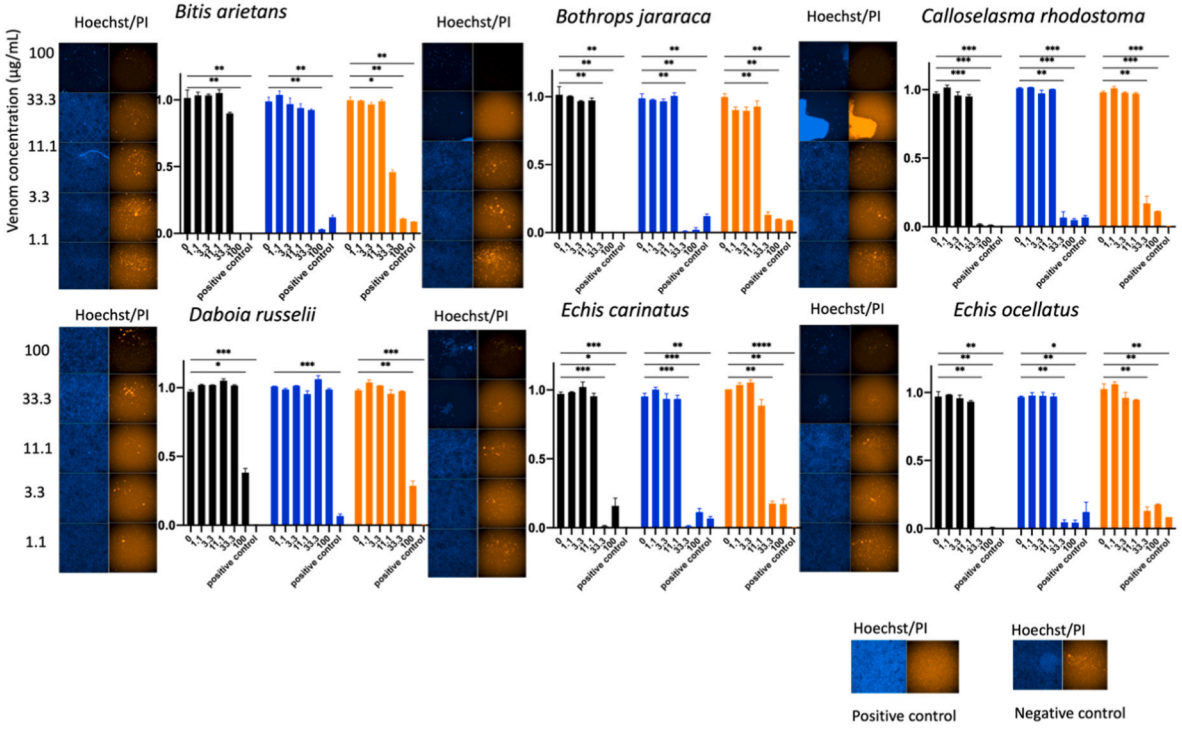

Fig. 4. Morphological images and three readouts for direct cytotoxicity assessment of crude venom on HaCat cells. Serial dilutions of the venoms (0, 1.1, 3.3, 11.1, 33.3, and 100 µg/mL) included in this study were investigated: black, ratio of live cell counts vs negative control (NC); blue, ratio of cell area vs NC; orange, ratio of resazurin reduction vs NC. Error bars show the mean ratio plus standard error. * highlights a statistically significant difference when compared to the negative control, PC represents the positive control, and PI means Propidium Iodide. Statistical testing was performed by two-way ANOVA, n = 3, *: p (Confidence Interval) < 0.05, **: $p < 0.005$, ***: $p < 0.0005$. All the bar chart share the same y-axis units, representing the ratio percentage (%) between the tested wells and the negative control wells.

nonspecific assay interference. Importantly, even under these sensitized conditions, cytotoxic activity was lost after RP-HPLC nanofractionation, supporting the conclusion that chromatographic conditions compromise toxin bioactivity.

In RPTEC/TERT1 cells, cytotoxicity was predominantly characterized by pronounced cell detachment and loss of monolayer integrity, rather than by strong reductions in metabolic activity or membrane permeability. RPTEC/TERT1 cell line is representative of renal tissue cells and could aid *in vitro* investigations of venoms that are known to be able to induce renal abnormalities (Sunitha et al., 2015). For example, the tight junction structure formed by RPTEC/TERT1 cells when damaged could mimic the *in vivo* loss of function of reabsorption or transportation of renal proximal tubule cells. We hypothesize that the RPTEC/TERT1 cell line is not as sensitive/tolerant to viper venoms as the HepaRG and iPSC-EC cell lines since envenoming by vipers often characterised by affecting the basement membrane and endothelial cells (Gutiérrez and Rucavado, 2000). While, the pronounced detachment observed in RPTEC/TERT1 cells suggests a specific vulnerability of renal epithelial cells to detachment-induced cell death mechanisms such as anoikis, highlighting a distinct cytotoxic response profile compared to the other cell types examined. Similar effects, including ECM degradation, were found by studies looking at skeletal muscle damage and important basement membrane proteins, with venom activity driven by the hydrolysis of cell-matrix components by SVMPs and/or hyaluronidases (Baldo et al., 2010; Bittenbinder et al., 2023a; Herrera et al., 2015). We observed that among the studied viper species, *D. russelii* was unique in its inability to degrade the ECM for all the tested cell lines. In consistency with our results, another study focusing on bioactivity showed that the venom of *D. russelii* (the same venom batch was used for this study) did not degrade a fluorescently labeled gelatin, which mimics ECM polymers such as collagen (Bittenbinder et al., 2023a). Previous studies about the mechanisms of permanent muscle damage by SVMPs showed enzymatical degradation of the collagen scaffold and other important basement membrane proteins (Williams et al., 2019), which is consistent with the ECM degradation observed in our HaCat cell line screening.

When comparing indirect and direct cytotoxic effects (Table S1), the most potent increase in cytotoxicity increase was observed for the iPSC-EC cell line, for which most of the venoms exhibited strongly enhanced indirect cytotoxicity. Only *D. russelii* venom did not induce ECM degradation in all the cell lines tested. For the RPTEC/TERT1 cell line, four venoms (*B. jararaca, C. rhodostoma, E. carinatus, and E. romani*) showed enhanced ECM degradation. Interestingly, *D. russelii* venom induced a significant disruption of the cell membrane in RPTEC/TERT1 cells, which was not observed for the direct cytotoxicity experiments. This effect might be the result of PLA_2 activity being enhanced by plasma phospholipid hydrolysis products, an effect which was previously observed in red blood cells (Saikia et al., 2013). Notably, the cytotoxicity profile of *Daboia russelii* differed from that of *Bothrops jararaca* and *Calloselasma rhodostoma*. In the crude venom screening, *D. russelii* induced marked reductions in live cell number and cellular metabolic activity across HepaRG, iPSC-EC, and HaCat cell lines, while no pronounced decrease in cell area was observed. This pattern suggests a predominance of direct cytotoxic effects rather than ECM-associated cell detachment. Given the known toxin composition of *D. russelii* venoms and our previous profiling studies, these effects are most plausibly associated with PLA_2-driven cytotoxic mechanisms rather than SVMP-mediated ECM degradation. A detailed investigation of intraspecific venom variation within *D. russelii* populations is beyond the scope of the present study. In HepaRG cells, the induced indirect cytotoxicity started from lower venom concentrations than the observed direct cytotoxicity and acted on cell permeability disruption, ECM degradation, and cell viability loss. With the iPSC-EC cell line, the three assay readouts were enhanced for all venoms investigated in the indirect cytotoxicity experiments compared to the direct. From this, we deduced that iPSC-EC cells were more sensitive to the induced cytotoxicity of viper venoms than other cell lines. In the HaCat cell line, enhanced effects caused by indirect cytotoxicity were only observed with the venom of *E. carinatus*, which affected measures of cell permeability disruption and ECM degradation.

Pronounced cell detachment and loss of monolayer integrity observed for several venoms are consistent with detachment-induced cell death mechanisms such as anoikis. Anoikis is triggered by disruption of cell-extracellular matrix interactions and represents a biologically relevant pathway in adherent cell systems. While the imaging-based readouts used in this study capture cell detachment and subsequent loss of viability, they do not allow unambiguous discrimination between anoikis and other forms of cell death. Definitive identification of anoikis would require targeted mechanistic assays, such as analysis of integrin signaling or apoptosis markers, which were beyond the scope of the present cytotoxicity profiling platform.

Because all cell models used in this study are adherent, pronounced loss of cell-matrix attachment and monolayer integrity is consistent with the involvement of detachment-induced cell death mechanisms such as anoikis. Anoikis is triggered by disruption of cell-extracellular matrix interactions and represents a biologically relevant response to venom-induced ECM damage. While the imaging-based assay panel captures cell detachment and subsequent loss of viability, it does not permit definitive discrimination between anoikis and other downstream cell death pathways. Further mechanistic resolution would require targeted assays beyond the scope of the present study.

3.2. Cytotoxicity profiling of nanofractionated venom toxins on the RPTEC/TERT1 cell line

RPTEC/TERT1 cells were seeded and cultured in 96 well plates until the wells were confluent. After that, cells were exposed to nanofractionated venom toxins and cytotoxicity quantified using the same assay readouts as performed for crude venom. The measured data was plotted into three bioactivity chromatograms and HT venomics data generated from fractions used to support toxin identifications, resulting in Protein Score Chromatograms (PSCs). Integrated cytotoxicity and toxin identification chromatograms were generated as three superimposed chromatographic representations (i.e., LC-UV, cytotoxicity chromatograms, and PSCs). Because of the scale of work required, we only used the RPTEC/TERT1 cell line to identify the cytotoxins. Toxin separations were ultimately performed by two different separation methods (i.e., RPLC and SEC). With RPLC, we screened the cytotoxicity of nanofractionated toxins of all the viper venoms for both direct and indirect cytotoxicity. As cytotoxicity observed for the crude venoms was lost after RPLC separation, we decided to apply SEC for venom separation for the representative venoms of *B. jararaca* and *C. rhodostoma*.

3.2.1. Nanofractionation analytics with RPLC for cytotoxicity profiling

The measured HPLC-UV chromatograms can be found in the supporting information in the document SI document of the HPLC UV chromatograms.PDF.

The direct and indirect cytotoxicity profiles of the RPLC separated venoms are presented in Fig. 5A and B, respectively. For the direct cytotoxic effects, no cytotoxicity peaks were found for any of the cytotoxicity readouts for all venoms tested. This could be the result of the requirement for multiple venom toxins to work in concert to induce cytotoxic effects or, more likely, is the result of toxin denaturation during separation. For the screening of indirect cytotoxicity effects by *C. rhodostoma* (the retention times of 23.7 and 27.5 min) and *D. russelii* (21.0, 25.0, 28.7, 30.5, 32.5, and 33.7 min), negative (bioactive) peaks were observed in the readout of live cell numbers. In addition, negative peaks were also observed in the readout of cell area for *C. rhodostoma* venom around the same retention times (23.7 and 27.5 min), indicating cytotoxins causing cell death and detachment. Cell viability was assessed by resazurin reduction; however, no cytotoxic effects were observed. No cytotoxicity peaks were observed in any of the cytotoxicity

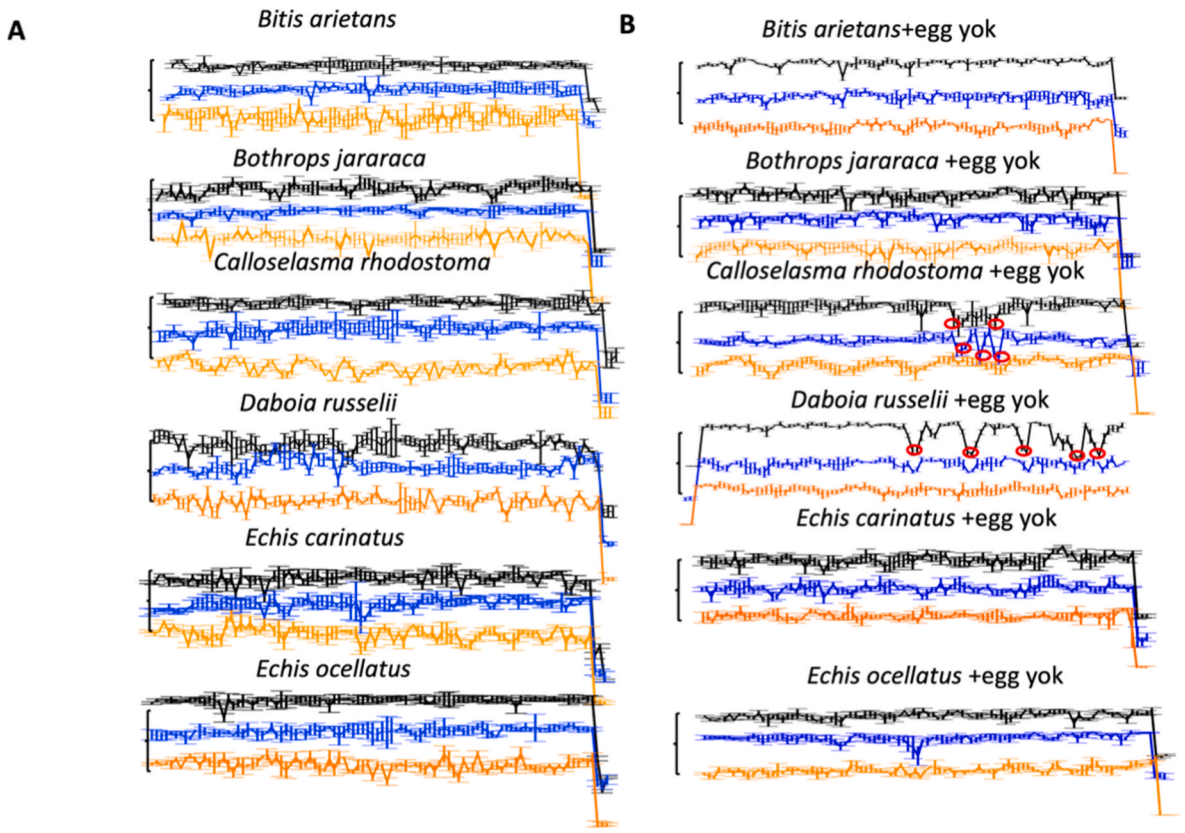

Fig. 5. Cytotoxicity screening of nanofractionated viper venoms on the RPTEC/TERT1 cell line. (A) Bioassay chromatograms showing the direct cytotoxic effects of separated and fractionated venom toxins of six viper venoms. (B) Bioassay chromatograms of the indirect cytotoxic effects of separated and fractionated venom toxins of six viper venoms. The black line indicates the ratio of live cell counts vs negative control. The blue line represents the ratio of cell area vs negative control. The orange line indicates the ratio of resazurin reduction. Red circles indicate the negative cytotoxicity peaks. Positive control was shown as a negative decrease on the right side (*D. russelii* on the left). All the bar chart share the same y-axis units, representing the ratio percentage (%) between the tested wells and the negative control wells.

readouts for any of the venoms tested, indicating no indirect cytotoxic effects. From these results, it was shown that some toxins, specifically indirect cytotoxins, survived the chromatographic separation intact. However, these findings suggest that nanofractionation analytics by RPLC for viper venoms likely results in considerable protein denaturation, rendering toxins inactive for cytotoxicity assaying.

Previously Xie et al. (2021) showed venom-induced cytotoxicity of erythrocytes by *C. rhodostoma* and *D. russelii* after reversed-phase separation. In this study and the study by Xie et al., PLA_2s were tentatively identified as the toxins responsible for the cytotoxicity observed. In this study, HT venomics identified PLA_2s with UniProt IDs of PA2HD_CALRH and PA2HD_CALRH for *C. rhodostoma* venom, and PA2B5_DABRR, PA2B3_DABRR, and PA2B8_DABRR for *D. russelii* venom in the fractions corresponding with the bioactive retention times. One logical explanation for the loss of cytotoxicity after RPLC is that larger venom toxins such as SVMPs largely or fully denature during RPLC separation because of the organic solvent acetonitrile used for separation (Bittenbinder et al., 2023b; Slagboom et al., 2020a; Xie et al., 2021) and/or due to the low pH of the eluents. Therefore, other chromatographic separation techniques should be investigated for usability within the current platform for post-column cytotoxicity profiling and bioactive toxin identification of viper snake venom cytotoxins.

3.2.2. *Nanofractionation analytics with SEC for cytotoxicity profiling*

As the direct cytotoxic activities were lost for all tested vipers when using RPLC, we investigated analytical SEC as a non-denaturing separation technique (Striegel et al., 2009). For this, we assessed the chromatographic cytotoxicity profile of two viper venoms separated by SEC and these venoms were also nanofractionated for HT venomics to identify responsible toxins.

3.2.2.1. Bothrops jararaca. For toxin identification, three notable peaks were observed in the LC-UV data (Fig. 6A). A broad negative peak was observed in the direct cytotoxicity chromatogram with a significant decrease in live cell number and cell area around the retention time frame from 9 to 13 min (Fig. 6B). As no differences in PI-stained cells were observed and no resazurin reduction changes were seen, the cytotoxicity mechanism of the broad negative peak was associated with ECM degradation. This manual identification was also concluded from the decrease in total cell number observed in the crude venom screening on RPTEC/TERT1 cells. The Protein Score Chromatograms (PSC) was correlated with the retention time frame of the negative peak (Fig. 6C). The first peak in the LC-UV data from 9 to 10 min was correlated to the first part of the broad cytotoxicity peak, which was assigned to closely co-eluting SVMPs (VM2J2_BOTJA, VM3H3_BOTJA, VM3B1_BOTJA, VM3B2_BOTJA). The second main peak in the LC-UV data around 10–11.6 min was assigned to VM3JA_BOTJA (SVMP) and to VSPH_BOTJA (SVSP). The third main peak in the LC-UV data from 11.6 to 13 min consisted of C-type lectin proteins (SLAA_BOTJA, SL1A_BOTJA, SLEA_BOTJA), an SVSP (VSP14_BOTJA), and VEGF (TXVE_BOTJA). Due to the limited resolution of analytical SEC and its separation principle being based on separation by toxin size, multiple toxins co-eluted (i.e., those belonging to the same toxin families) around the same retention time regions. Many studies on snake venoms have shown that SVMPs can induce ECM degradation by hydrolyzing key peptide bonds in the basement membrane (BM) and supporting ECM, promoting the weakening of the mechanical stability of the BM (Araki

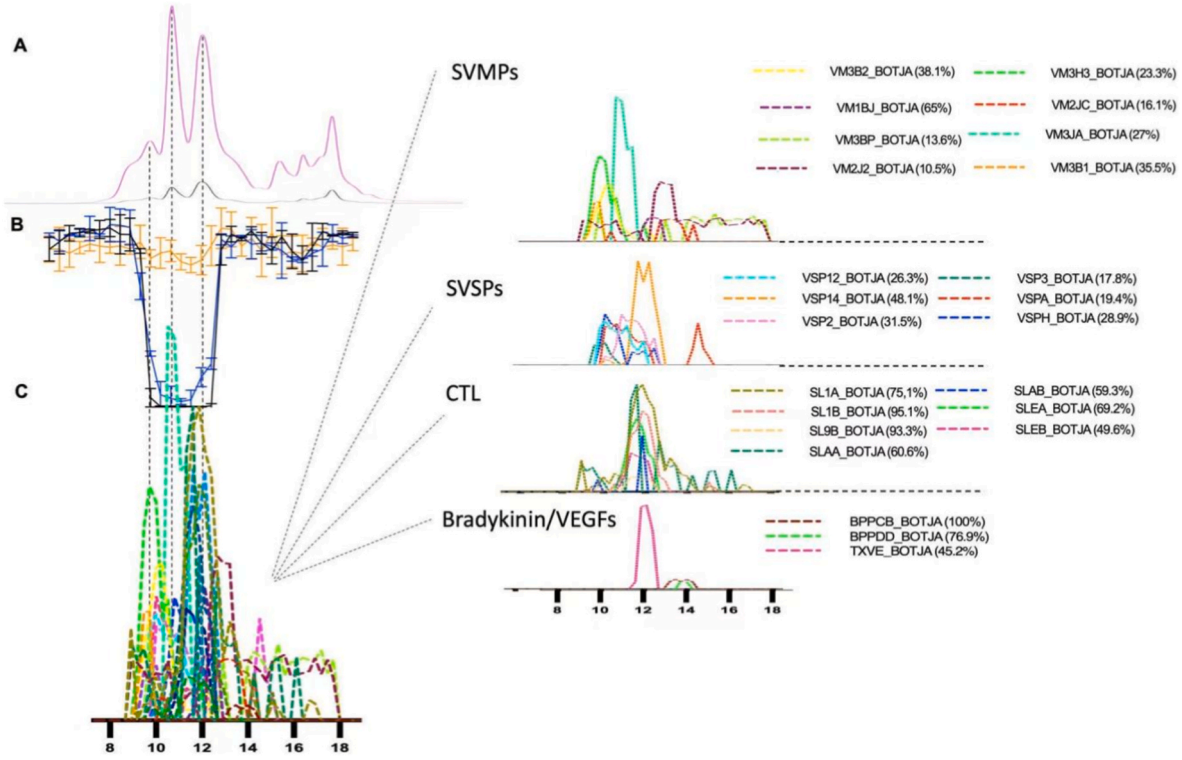

Fig. 6. Cytotoxicity profiling chromatogram of size-exclusion chromatography (SEC)-nanofractioned venom of *B. jararaca*. (A) SEC-ultraviolet (UV) traces of separated snake venom toxins at 220 nm (black) and 254 nm (purple). (B) Direct cytotoxicity chromatogram obtained from the readouts of the three cytotoxicity assays on the RPTEC/TERT1 cell line. The black, blue, and orange chromatograms indicate the ratio of live cell number counting, cell area, and resazurin reduction versus negative control, respectively. (C) Protein Score Chromatograms (PSCs) acquired from the High throughput (HT) Venomics data. For the PSCs, results from Mascot searches using species-specific databases. (%) means toxin sequence coverage. All the cytotoxicity chromatograms share the same y-axis units, representing the ratio percentage (%) between the tested wells and the negative control wells, as well as the same x-axis units given in the legend and in the figure, representing retention time in minutes (min).

et al., 2002; Bittenbinder et al., 2023a; Escalante et al., 2011; Gutiérrez et al., 2006). As for SVSPs and CTLs, these toxins are typically associated with affecting haemostasis by modulating the coagulation cascade via fibrinogenolysis or interacting with platelets (Arlinghaus and Eble, 2012; Serrano, 2013), while VEGF is a vital regulator for vascular network formation (Toivanen et al., 2017). In conclusion, *B. jararaca* venom-induced ECM degradation in RPTEC/TERT1 cells likely has a close relationship with SVMPs, whereas other toxins might serve an auxiliary role in the cytotoxicity profile observed.

The use of a column temperature of 30 °C during RP-HPLC represents a compromise between chromatographic performance and preservation of toxin structure. While RP-HPLC can induce partial denaturation of some venom proteins, particularly larger SVMPs, moderate temperature combined with gradient elution improves separation efficiency and does not, by itself, account for the observed loss of cytotoxic activity, which is more likely driven by exposure to organic solvent and acidic mobile phase conditions.

3.2.2.2. Calloselasma rhodostoma. In Fig. 7A, the LC-UV data were listed. In subsequence, we observed two substantial negative peaks in the direct cytotoxicity chromatogram data (Fig. 7B), which represented ECM degradation and no cell permeability disruption (because of no PI-stained cells). Also, no altered cell viability was observed, which correlated with the screening of crude venom on RPTEC/TERT1 cells. For toxin identification, unlike the results from *B. jararaca* venom, the bioactivity peaks presented better resolution with fewer co-eluting toxins per peak. The first peak (11.6–12.1 min) correlated to the SVMP VM2RH_CALRH (SVMP), while the second (broader) peak (12.1–13.8 min) and was correlated to the SVMP VM1K_CALRH (SVMP). It was thus found that SVMPs contributed to the observed direct cytotoxicity caused by *C. rhodostoma* venom in the RPTEC/TERT1 cell line.

SEC-nanofractionation preserved cytotoxic activity but yielded fractions containing mixtures of venom toxins belonging to multigenic families, including SVMPs, PLA_2 toxins, and CTLs. Within these families, distinct subclasses (such as PI and PIII-SVMPs, catalytically active and inactive PLA_2 homologs, and multimeric CTLs) are known to differ in their biological activities. Although individual toxin subclasses cannot be resolved by SEC alone, the observed cytotoxicity profiles are consistent with known functional properties of these toxin families. Definitive assignment of cytotoxic effects to specific toxin subclasses would require purification of individual toxins and/or the use of selective inhibitors, which represents an avenue for future investigation.

4. Conclusion

This project optimized and applied nanofractionation analytics for cytotoxicity screening of viper venoms on four mammal cell lines that mimic *in vitro* different tissues that are potentially affected during snakebite envenoming. The previously developed approach of high-throughput *in vitro* bioassay screening was applied to investigate the activity of six crude viper venoms on the RPTEC/TERT1, HepaRG, iPSC-EC, and HaCat cell lines. Selective cytotoxicity was observed between RPTEC/TERT1 (ECM degradation) and the other cell lines (disruption of cell permeability, ECM degradation, and cell viability loss), which highlights differences in sensitivity to viper venoms among the cell lines. The cytotoxicity responses (cell permeability, ECM degradation, cell metabolism) were generally intensified in the presence of egg yolk emulsion for all venoms tested. Robust cytotoxic peaks align with extracellular matrix (ECM)-associated cytotoxicity, which is evidenced

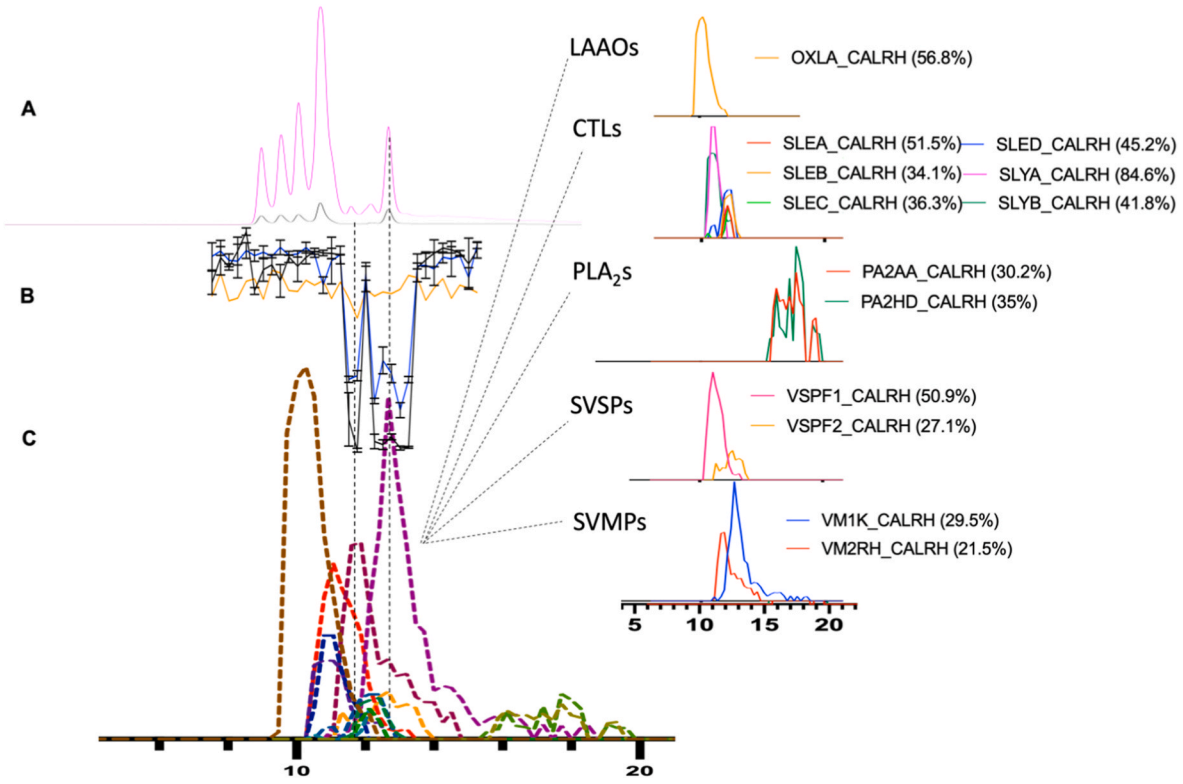

Fig. 7. Cytotoxicity profiling chromatogram of size-exclusion chromatography (SEC)-nanofractioned venom of *C. rhodostoma*. (A) SEC-ultraviolet (UV) traces of separated snake venom toxins at 220 nm (black) and 254 nm (purple). (B) Direct cytotoxicity chromatogram obtained from the readouts of the three cytotoxicity assays on the RPTEC/TERT1 cell line. The black, blue, and orange chromatograms indicate the ratio of live cell number counting, cell area, and resazurin reduction versus negative control, respectively. (C) Protein Score Chromatograms (PSCs) acquired from the High throughput (HT) Venomics data. For the PSCs, results from Mascot searches using species-specific databases. (%) means toxin sequence coverage. All the cytotoxicity chromatograms share the same y-axis units, representing the ratio percentage (%) between the tested wells and the negative control wells, as well as the same x-axis units given in the legend and in the figure, representing retention time in minutes (min).

by marked decreases in cell area and compromised monolayer integrity. Downstream use of nanofractionation analytics following two orthogonal chromatographic separation methods, and coupled with HT venomics, permitted investigation and identification of aetiological venom toxins, with SVMPs seemingly key components. Given that cytotoxicity is one of the most common pathological toxicities associated with viper envenomings and contributes to important local pathology around the bite site that frequently results in morbidity, the results presented here highlight how our analytical approach can provide a better understanding of the cytotoxicity of viper venoms at the toxin level. This research could prove valuable by aiding in the design and development of next-generation snakebite treatments by focusing on the neutralization of specific cytotoxins found in diverse viper venoms.

CRediT authorship contribution statement

Haifeng Xu: Writing – review & editing, Writing – original draft, Validation, Funding acquisition, Data curation, Conceptualization. **Mátyás A. Bittenbinder:** Writing – review & editing, Validation, Methodology, Conceptualization. **Julien Slagboom:** Writing – review & editing, Validation, Methodology. **Nicholas R. Casewell:** Writing – review & editing, Validation. **Paul Jennings:** Writing – review & editing. **Jeroen Kool:** Writing – review & editing, Validation, Supervision, Project administration, Funding acquisition, Conceptualization.

Ethical statement

The authors declare that no ethical issues are associated with this study. The research did not involve human participants, vertebrate animals, or endangered species, and no *in vivo* experiments were conducted. All experimental work was performed in compliance with institutional and international guidelines for good scientific practice.

Declaration of competing interest

None of the authors (Haifeng Xu, Mátyás A. Bittenbinder, Julien Slagboom, Nicholas R. Casewell, Paul Jennings, and Jeroen Kool) declare a competing interest.

Acknowledgments

We appreciate Daniel Da Costa Pereira, Elisabeth Naderlinger, and Liliana Capinha of the Division of Molecular and Computational Toxicology for their help and advice on the cell culturing aspects of this study. This research was funded by the China Scholarship Council (File No. 202003250087).

The LC-MS/MS data generated and used in this study as well as the high-content imaging datasets has been deposited in the public data repository XXXXX with accession number: ABCDE.

Appendix A. Supplementary data

Supplementary data to this article can be found online at https://doi.org/10.1016/j.toxicon.2025.108969.

Data availability

The LC-MS/MS data generated and used in this study as well as the

high-content imaging datasets have been deposited in the public data repository Zenado accessible via the following link: https://zenodo.org/records/18266356.

References

Aglanu, L.M., Amuasi, J.H., Duah, I.K., Agbogbatey, M.K., Steinhorst, J., Adobasom-Anane, A.G., Bukari, Z., Azabu, T.J., Kreuels, B., Lalloo, D.G., et al., 2025. Clinical presentation and management of snakebite envenoming in northern Ghana. PLoS Neglected Trop. Dis. 19, e0013820.

Aleshin, V.A., Artiukhov, A.V., Oppermann, H., Kazantsev, A.V., Lukashev, N.V., Bunik, V.I., 2015. Mitochondrial impairment May increase cellular NAD(P)H: resazurin oxidoreductase activity, perturbing the NAD(P)H-based viability assays. Cells 4, 427–451.

Almeida, T., Priante, S.P., João, G.P., Nery Oliveira, D., Mouta, G., Sachett, J., de Lima Ferreira, L.C., Oliveira de Amorim, R.L., Lobo, L., Sartim, M.A., et al., 2025. Strokes following snakebite envenomations: a systematic review and individual patient data meta-analysis. PLoS Neglected Trop. Dis. 19, e0013789.

Araki, S., Masuda, S., Maeda, H., Ying, M.J., Hayashi, H., 2002. Involvement of specific integrins in apoptosis induced by vascular apoptosis-inducing protein 1. Toxicon 40, 535–542.

Arlinghaus, F.T., Eble, J.A., 2012. C-type lectin-like proteins from snake venoms. Toxicon 60, 512–519.

Aschauer, L., Gruber, L.N., Pfaller, W., Limonciel, A., Athersuch, T.J., Cavill, R., Khan, A., Gstraunthaler, G., Grillari, J., Grillari, R., et al., 2013. Delineation of the key aspects in the regulation of epithelial monolayer formation. Mol. Cell Biol. 33, 2535–2550.

Avella, I., Schulte, L., Damm, M., Uhrig, L., Cabrera-Orefice, A., Eichberg, J., Hardes, K., Hurka, S., Lindner, T., Vilcinskas, A., et al., 2025. Venomics of the Arabian saw-scaled viper (Echis coloratus) through transcriptome-guided proteomics and in vitro functional profiling. PLoS Neglected Trop. Dis. 19, e0013439.

Baldo, C., Jamora, C., Yamanouye, N., Zorn, T.M., Moura-da-Silva, A.M., 2010. Mechanisms of vascular damage by hemorrhagic snake venom metalloproteinases: tissue distribution and in situ hydrolysis. PLoS Neglected Trop. Dis. 4, e727.

Bittenbinder, M.A., Bergkamp, N.D., Slagboom, J., Bebelman, J.P.M., Casewell, N.R., Siderius, M.H., Smit, M.J., Kool, J., Vonk, F.J., 2023a. Monitoring snake venom-induced extracellular matrix degradation and identifying proteolytically active venom toxins using fluorescently labeled substrates. Biology 12, 765.

Bittenbinder, M.A., Capinha, L., Da Costa Pereira, D., Slagboom, J., van de Velde, B., Casewell, N.R., Jennings, P., Kool, J., Vonk, F.J., 2023b. Development of a high-throughput in vitro screening method for the assessment of cell-damaging activities of snake venoms. PLoS Neglected Trop. Dis. 17, e0011564.

Bode, K.J., Mueller, S., Schweinlin, M., Metzger, M., Brunner, T., 2019. A fast and simple fluorometric method to detect cell death in 3D intestinal organoids. Biotechniques 67, 23–28.

Bustillo, S., Garcia-Denegri, M.E., Gay, C., Van de Velde, A.C., Acosta, O., Angulo, Y., Lomonte, B., Gutierrez, J.M., Leiva, L., 2015. Phospholipase A(2) enhances the endothelial cell detachment effect of a snake venom metalloproteinase in the absence of catalysis. Chem. Biol. Interact. 240, 30–36.

Casewell, N.R., Jackson, T.N.W., Laustsen, A.H., Sunagar, K., 2020. Causes and consequences of snake venom variation. Trends Pharmacol. Sci. 41, 570–581.

Christensen, K., Roudnicky, F., Burcin, M., Patsch, C., 2019. Monolayer generation of vascular endothelial cells from human pluripotent stem cells. Methods Mol. Biol. 1994, 17–29.

Du, X.Y., Sim, D.S., Lee, W.H., Zhang, Y., 2006. Blood cells as targets of snake toxins. Blood Cells Mol. Dis. 36, 414–421.

Escalante, T., Ortiz, N., Rucavado, A., Sanchez, E.F., Richardson, M., Fox, J.W., Gutierrez, J.M., 2011. Role of collagens and perlecan in microvascular stability: exploring the mechanism of capillary vessel damage by snake venom metalloproteinases. PLoS One 6, e28017.

Gutierrez, J.M., Calvete, J.J., Habib, A.G., Harrison, R.A., Williams, D.J., Warrell, D.A., 2017. Snakebite envenoming. Nat. Rev. Dis. Primers 3, 17063.

Gutiérrez, J.M., Calvete, J.J., Habib, A.G., Harrison, R.A., Williams, D.J., Warrell, D.A., 2017. Snakebite envenoming. Nat. Rev. Dis. Primers 3, 1–21.

Gutiérrez, J.M., Escalante, T., Rucavado, A., Herrera, C., 2016. Hemorrhage caused by snake venom metalloproteinases: a journey of discovery and understanding. Toxins 8, 93.

Gutiérrez, J.M., Núñez, J., Escalante, T., Rucavado, A., 2006. Blood flow is required for rapid endothelial cell damage induced by a snake venom hemorrhagic metalloproteinase. Microvasc. Res. 71, 55–63.

Gutiérrez, J.M., Rucavado, A., 2000. Snake venom metalloproteinases: their role in the pathogenesis of local tissue damage. Biochimie 82, 841–850.

Gutiérrez, J.M., Rucavado, A., Escalante, T., Díaz, C., 2005. Hemorrhage induced by snake venom metalloproteinases: biochemical and biophysical mechanisms involved in microvessel damage. Toxicon 45, 997–1011.

Harrison, R.A., Hargreaves, A., Wagstaff, S.C., Faragher, B., Lalloo, D.G., 2009. Snake envenoming: a disease of poverty. PLoS Neglected Trop. Dis. 3, e569.

Herrera, C., Escalante, T., Voisin, M.B., Rucavado, A., Morazan, D., Macedo, J.K., Calvete, J.J., Sanz, L., Nourshargh, S., Gutierrez, J.M., et al., 2015. Tissue localization and extracellular matrix degradation by PI, PII and PIII snake venom metalloproteinases: clues on the mechanisms of venom-induced hemorrhage. PLoS Neglected Trop. Dis. 9, e0003731.

Hofmann, E.P., Rautsaw, R.M., Strickland, J.L., Holding, M.L., Hogan, M.P., Mason, A.J., Rokyta, D.R., Parkinson, C.L., 2018. Comparative venom-gland transcriptomics and venom proteomics of four sidewinder rattlesnake (Crotalus cerastes) lineages reveal little differential expression despite individual variation. Sci. Rep. 8, 15534.

Lin, J.-H., Sung, W.-C., Mu, H.-W., Hung, D.-Z., 2022. Local cytotoxic effects in cobra envenoming: a pilot study. Toxins 14, 122.

López-Dávila, A.J., Weber, N., Kraft, T., Matinmehr, F., Arias-Hidalgo, M., Fernández, J., Lomonte, B., Gutiérrez, J.M., 2021. Cytotoxicity of snake venom Lys49 PLA2-like myotoxin on rat cardiomyocytes ex vivo does not involve a direct action on the contractile apparatus. Sci. Rep. 11, 19452.

Mladic, M., Zietek, B.M., Iyer, J.K., Hermarij, P., Niessen, W.M., Somsen, G.W., Kini, R. M., Kool, J., 2016. At-line nanofractionation with parallel mass spectrometry and bioactivity assessment for the rapid screening of thrombin and factor Xa inhibitors in snake venoms. Toxicon 110, 79–89.

Saikia, D., Majumdar, S., Mukherjee, A.K., 2013. Mechanism of in vivo anticoagulant and haemolytic activity by a neutral phospholipase A(2) purified from Daboia russelii russelii venom: correlation with clinical manifestations in Russell's Viper envenomed patients. Toxicon 76, 291–300.

Selinummi, J., Ruusuvuori, P., Podolsky, I., Ozinsky, A., Gold, E., Yli-Harja, O., Aderem, A., Shmulevich, I., 2009. Bright field microscopy as an alternative to whole cell fluorescence in automated analysis of macrophage images. PLoS One 4, e7497.

Serrano, S.M., 2013. The long road of research on snake venom serine proteinases. Toxicon 62, 19–26.

Slagboom, J., Derks, R.J.E., Sadighi, R., Somsen, G.W., Ulens, C., Casewell, N.R., Kool, J., 2023. High-throughput venomics. J. Proteome Res. 22, 1734–1746.

Slagboom, J., Mladic, M., Xie, C., Kazandjian, T.D., Vonk, F., Somsen, G.W., Casewell, N. R., Kool, J., 2020a. High throughput screening and identification of coagulopathic snake venom proteins and peptides using nanofractionation and proteomics approaches. PLoS Neglected Trop. Dis. 14, e0007802.

Slagboom, J., Mladić, M., Xie, C., Kazandjian, T.D., Vonk, F., Somsen, G.W., Casewell, N. R., Kool, J., 2020b. High throughput screening and identification of coagulopathic snake venom proteins and peptides using nanofractionation and proteomics approaches. PLoS Neglected Trop. Dis. 14, e0007802.

Still, K.B.M., Slagboom, J., Kidwai, S., Xie, C., Zhao, Y., Eisses, B., Jiang, Z., Vonk, F.J., Somsen, G.W., Casewell, N.R., et al., 2020. Development of high-throughput screening assays for profiling snake venom phospholipase A(2) activity after chromatographic fractionation. Toxicon 184, 28–38.

Striegel, A.M., Yau, W.W., Kirkland, J.J., Bly, D.D., 2009. Modern Size-Exclusion Liquid Chromatography. John Wiley & Sons, Inc.

Sunitha, K., Hemshekhar, M., Thushara, R.M., Santhosh, M.S., Sundaram, M.S., Kemparaju, K., Girish, K.S., 2015. Inflammation and oxidative stress in viper bite: an insight within and beyond. Toxicon 98, 89–97.

Szentesi, P., Magyar, Z.É., Fernández, J., Csernoch, L., Ruiz-Campos, M., Lomonte, B., Gutiérrez, J.M., Lopez-Dávila, A.J., 2025. Myotoxin II, a snake venom Lys49 phospholipase A2 homolog, induces activation of the ryanodine receptor in artificial bilayers. Toxicon 267, 108590.

Tasoulis, T., Isbister, G.K., 2017. A review and database of snake venom proteomes. Toxins 9, 290.

Toivanen, P.I., Nieminen, T., Laakkonen, J.P., Heikura, T., Kaikkonen, M.U., Ylä-Herttuala, S., 2017. Snake venom VEGF Vammin induces a highly efficient angiogenic response in skeletal muscle via VEGFR-2/NRP specific signaling. Sci. Rep. 7, 5525.

Wachtel, E., Bittenbinder, M.A., van de Velde, B., Slagboom, J., de Monts de Savasse, A., Alonso, L.L., Casewell, N.R., Vonk, F.J., Kool, J., 2023. Application of an extracellular matrix-mimicking fluorescent polymer for the detection of proteolytic venom toxins. Toxins 15, 294.

Wieser, M., Stadler, G., Jennings, P., Streubel, B., Pfaller, W., Ambros, P., Riedl, C., Katinger, H., Grillari, J., Grillari-Voglauer, R., 2008. hTERT alone immortalizes epithelial cells of renal proximal tubules without changing their functional characteristics. Am. J. Physiol. Ren. Physiol. 295, F1365–F1375.

Williams, D.J., Gutierrez, J.M., Calvete, J.J., Wuster, W., Ratanabanangkoon, K., Paiva, O., Brown, N.I., Casewell, N.R., Harrison, R.A., Rowley, P.D., et al., 2011. Ending the drought: new strategies for improving the flow of affordable, effective antivenoms in Asia and Africa. J. Proteonomics 74, 1735–1767.

Williams, H.F., Mellows, B.A., Mitchell, R., Sfyri, P., Layfield, H.J., Salamah, M., Vaiyapuri, R., Collins-Hooper, H., Bicknell, A.B., Matsakas, A., et al., 2019. Mechanisms underpinning the permanent muscle damage induced by snake venom metalloprotease. PLoS Neglected Trop. Dis. 13, e0007041.

Willinger, C.C., Thamaree, S., Schramek, H., Gstraunthaler, G., Pfaller, W., 1995. In vitro nephrotoxicity of Russell's viper venom. Kidney Int. 47, 518–528.

Xie, C., Bittenbinder, M.A., Slagboom, J., Arrahman, A., Bruijns, S., Somsen, G.W., Vonk, F.J., Casewell, N.R., Garcia-Vallejo, J.J., Kool, J., 2021. Erythrocyte haemotoxicity profiling of snake venom toxins after nanofractionation. J. Chromatogr., B: Anal. Technol. Biomed. Life Sci. 1176, 122586.

Xu, H., Bittenbinder, M.A., Slagboom, J., Casewell, N.R., Jennings, P., Kool, J., 2025. Profiling cytotoxicity of nanofractionated elapid snake venoms in human cell lines representing different tissues. J. Pharm. Anal., 101398

Zietek, B.M., Mayar, M., Slagboom, J., Bruyneel, B., Vonk, F.J., Somsen, G.W., Casewell, N.R., Kool, J., 2018. Liquid chromatographic nanofractionation with parallel mass spectrometric detection for the screening of plasmin inhibitors and (metallo)proteinases in snake venoms. Anal. Bioanal. Chem. 410, 5751–5763.